A model-based failure times identification for a system governed by a 2D parabolic partial differential equation

Mohamed Salim Bidou, Laetitia Perez, Sylvain Verron, Laurent Autrique

Received: 29 August 2023 | Revised: 24 November 2023 | Accepted: 13 March 2024

IET Control Theory & Applications

DOI: 10.1049/cth2.12652

The Institution of Engineering and Technology WILEY

ORIGINAL RESEARCH

A model-based failure times identification for a system governed by a 2D parabolic partial differential equation

Mohamed Salim Bidou | **Laetitia Perez** | **Sylvain Verron** | **Laurent Autrique**

LARIS, Polytech, University of Angers, Angers, France

Correspondence
Mohamed Salim Bidou, LARIS, Polytech, University of Angers, France.
Email: mohamedsalim.bidou@univ-angers.fr

Abstract

This research focuses on the identification of failure times in thermal systems governed by partial differential equations, a task known for its complexity. A new model-based diagnostic approach is presented that aims to accurately identify failing heat sources and accurately determine their failure times, which is crucial when multiple heat sources fail and there is a delay in detection by distant sensors. To validate the effectiveness of the approach, a comparative analysis is carried out with an established method based on a Bayesian filter, the Kalman filter. The aim is to provide a comprehensive analysis, highlighting the advantages and potential limitations of the methodology. In addition, a Monte Carlo simulation is implemented to assess the impact of sensor measurements on the performance of this new approach.

1 | INTRODUCTION

In recent years, there has been an increasing interest in fault diagnosis due to the growing complexity and safety concerns of industrial systems. To model various phenomena in complex physical systems, theories based on partial differential equations (PDEs) have gained popularity. For instance, the use of Fourier's law in thermal sciences, which governs heat exchange, leads to a system of parabolic PDEs. Ordinary differential equations (ODEs) alone are insufficient to accurately capture the dynamic behaviors of most practical engineering models, as they have limited ability to account for spatial and temporal evolution.

To address these challenges, model-based fault detection and diagnosis systems have emerged as a prominent approach. In industrial heating systems, failures in heating sources can lead to decreased efficiency, product quality issues, and safety hazards. Accurate identification of failure times is crucial in heating, ventilation, air conditioning (HVAC) systems and condensing boilers [1, 2] to ensure temperature consistency, energy efficiency, and occupant comfort. Power generation plants heavily rely on heating sources, and any faults can result in power outages or reduced capacity. Similarly, solar thermal systems, which utilize sunlight as a heating source, require reliable fault detection to maximize energy output. In process industries such as petrochemical plants or food processing facilities, thermal systems play a vital role, and timely fault detection is essential for maintaining production schedules, ensuring product quality, and preventing safety risks.

The field of controlling and estimating of PDEs has been a subject of extensive research for several decades. Two main approaches have been explored in PDEs control and estimation: (i) Early lumping, which involves approximating the PDEs with ordinary differential equations (ODEs) and conducting the design in a finite-dimensional space, as discussed in previous studies [3, 4]; and (ii) Late lumping, which focuses on designing in an infinite-dimensional space and directly studying the PDEs without using approximate methods, as investigated in other research works [5, 6].

While significant attention has been given to control and estimation research in the context of PDEs, the field of system fault diagnosis in PDEs has received relatively less exploration. Existing diagnostic schemes for PDEs primarily rely on early lumping approaches [7–11]. However, this approach has certain limitations. The finite-dimensional approximation often leads to the loss of essential intrinsic characteristics present in the original PDEs model. On the other hand, "late lumping" methods based on PDEs observer-based fault diagnosis schemes have been successfully applied to parabolic systems in various research projects, such as those mentioned in references [12–18]. These approaches aim to address the drawbacks of early lumping methods and provide more accurate fault

diagnosis by directly considering the inherent characteristics of the PDEs model.

In the context of parametric identification, the search for faults in a system modeled by a set of partial differential equations (PDEs) can be considered an inverse problem [19]. Inverse Heat Conduction Problems (IHCPs) are widely used in various engineering domains, particularly in thermal engineering. However, IHCPs are mathematically ill-posed, as it is challenging to satisfy the requirements of existence, uniqueness, and continuity simultaneously. This ill-posedness is exacerbated by the sensitivity of IHCPs to random errors in measurement, leading to significant inaccuracies in the numerical solutions. Several methods have been proposed to tackle IHCPs, including the Tikhonov regularization method [20, 21], the sequential function specification method [22, 23], the iterative regularization method [24, 25] and the Bayesian methods [26, 27].

In [28], an iterative conjugate gradient regularization approach was utilized to determine the heat transfer coefficient (HTC) in a two-dimensional transient heat conduction scenario. Similarly in [29], the same method was applied to predict the HTC at the inner wall of a nuclear power plant pipeline responsible for transporting a mixture of warm and cold fluids. Another study conducted by [30], focused on the estimation of surface heat flux in three-dimensional IHCP. Additionally, [31] proposed an adaptive selection of relevant sensors within a network was proposed to estimate an unknown mobile heating flux, optimizing the sensor configuration to enhance the accuracy of the estimation. Furthermore, in [32], a novel data-driven structure was introduced to enable direct analysis and parameter inversion of heat conduction problems (HCPs). This approach leverages available data to directly infer the parameters of the heat conduction model, facilitating efficient analysis and estimation.

When it comes to the identification of failure times in a system governed by PDEs, the failure instants within the thermal framework can be identified by solving IHCPs based on observations from the malfunctioning system. However, it is crucial to address some important considerations in the fault diagnosis process. First, IHCPs are highly sensitive to measurement errors due to their ill-posed nature [33]. Additionally, the failures being investigated are characterized as "on-off" events, and the study's structure shares similarities with hybrid systems that involve delays caused by discontinuous switching associated with heat transport phenomena.

In a recent study [19], we have proposed an approach to effectively identify failures in one or more heat sources based on noisy observations. Our method allows for precise identification of failing heat sources, accurate determination of failure times, and the potential for restoration to normal operation. The identification procedure is formulated as a quadratic criterion minimization problem and solved using an iterative regularization method. To assess the effectiveness of our approach, we compare it with another Bayesian filter-based method, specifically the Kalman filter, which was also developed in our recent study [34]. This comparative analysis aims to provide a comprehensive evaluation, highlighting the advantages and disadvantages of our recent approach.

FIGURE 1 Positions of the plate's 3 sources and 4 sensors.

The structure of this article is organized as follows. Section 2 provides a detailed description of the physical problem formulation in a two-dimensional geometry. In Section 3, a conjugate gradient iterative regularization method has been developed and implemented. Particular attention is paid to the definition of the failure and restart instants of heating sources. The inverse problem is then presented. Its resolution requires the iterative determination of the temperature, the gradient of the criterion and the depth of the descent. Section 4 presents the Bayesian filter to estimate the intensity of the heating sources based on the Kalman filter and smoother, followed by a methodology that allows the estimation of failure and restart instants based on candidate search strategies and signals from the heating sources. Numerical results are presented and discussed in Section 5. Finally, Section 6 presents the conclusion and the perspectives offered by this work.

2 | APPLICATION DESCRIPTION

2.1 | The direct problem

The application given here is a 1 meter long by 1 meter wide by 2 mm thick aluminum plate. On this are positioned four temperature sensors and three heating sources. The locations of the three sources and four sensors are known (Figure 1). The behavior of the heating sources is unpredictable. These, specifically, will encounter all-or-nothing failures. Consequently, a source may stop operating (in which case its heat flow would be zero) and then return to its regular behavior, and this could occur frequently.

The geometric domain is defined as $\Omega = [-0.5, 0.5]^2 \subset \Re^2$, every point in space possesses its own coordinates $(x, y) \in \Omega$. $t \in [0, t_f]$ is the time variable. $T(x, y, t)$ represents the temperature at every point in space. The following set of mathematical

TABLE 1 Mathematical model input parameters.

Symbol	Definition	Values
ρc	Volumetric heat	$2.421.10^6$ J · m^{-3} · K^{-1}
h	Natural convection coefficient	10 W · m^{-2} · K^{-1}
λ	Thermal conductivity	178 W · m^{-1} · K^{-1}
T_0	Initial temperature	293 K
t_f	Final time	3600 s
e	Thickness	$2 \cdot 10^{-3}$ m

equations [35] describes the temperature's temporal evolution in the Ω domain:

$$\begin{cases} \rho C \dfrac{\partial T(x,y,t)}{\partial t} - \lambda \Delta T(x,y,t) \\ \qquad\qquad = \dfrac{\Phi(x,y,t) - 2h(T(x,y,t) - T_0)}{e}, \\ T(x,y,0) = T_0, \quad (x,y) \in \Omega, \\ -\lambda \dfrac{\partial T(x,y,t)}{\partial \vec{n}} = 0, \quad (x,y,t) \in \Gamma \times [0, t_f], \end{cases} \tag{1}$$

The model's input parameters are presented in Table 1. By utilizing the finite element method, the direct problem described by equations (1) can be solved numerically when all input parameters of the model are determined using the Comsol-Multiphysics software integrated with Matlab (Figure 3).

The total amount of heat flux $\Phi(x,y,t)$ is determined by the collective contribution of several distinct heating sources. Mathematically, the heat flux at a given point (x,y,t) is the sum of individual heat fluxes generated by each source, denoted as $\Phi_i(x,y,t)$, where i ranges from 1 to n_{heat}:

$$\Phi(x,y,t) = \sum_{i=1}^{n_{\text{heat}}} \Phi_i(x,y,t), \quad \text{with: } n_{\text{heat}} = 3. \tag{2}$$

These heat sources exhibit spatially varying distributions and temporal characteristics. Each heat source, $\Phi_i(x,y,t)$, can be described by the product of three separate functions:

$$\Phi_i(x,y,t) = f_i(x,y) g_i(t) \chi_i(t). \tag{3}$$

The function $f_i(x,y)$ is pivotal in defining the spatial support and distribution of each heat source within the system. To accurately model this, we employ a Gaussian distribution centered around the point (x_i, y_i), where each heat source is located. The equation is formulated as follows:

$$f_i(x,y) = \exp\left(-\frac{(x - x_i)^2 + (y - y_i)^2}{(5 \times 10^{-2})^2} \right). \tag{4}$$

The standard deviation 5×10^{-2} is a key parameter that influences the spatial extent of heat dispersion from each source. A smaller variance value would result in a more localized heat distribution, creating a steeper gradient around the source, while a larger variance would lead to a more widespread, gradual distribution of heat. The chosen variance value for our model is designed to realistically represent the physical dispersion characteristics of heat within the system, carefully balancing the need for accurate portrayal of the heat's localized impact and ensuring that the distribution is sufficiently extensive to cover the relevant areas of the system [36, 37].

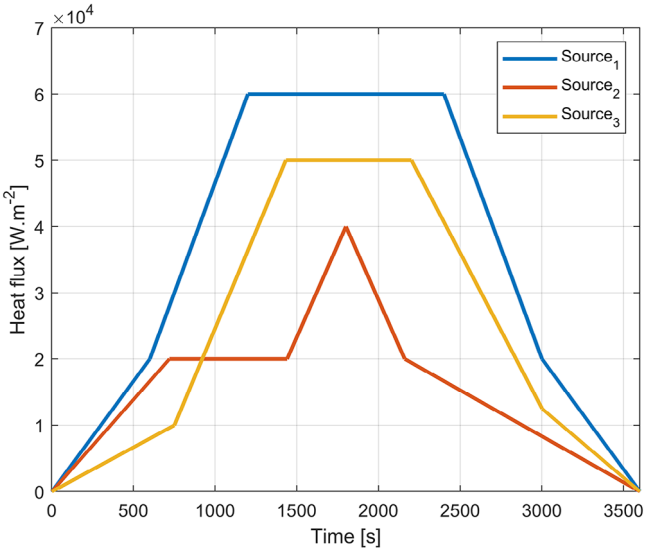

FIGURE 2 Flux $g_1(t)$, $g_2(t)$ and $g_3(t)$ of the three sources.

The temporal behavior of each heat source is captured by the function $g_i(t)$, which represents the normal heating flux generated by the source i. This function provides information about how the heat flux varies over time for each individual source. To provide a visual representation of the heat flux dynamics, Figure 2 displays the evolution of the heat flux for the three sources over time. Furthermore, the function $\chi_i(t)$ is introduced to account for potential faults or failures in the heating source i:

$$\chi_i(t) = \begin{cases} 1 & \text{without failure,} \\ 0 & \text{in case of failure.} \end{cases} \tag{5}$$

It serves as an indicator function, assuming a value of 1 when the source is operating without any failure and 0 in the event of a failure. The occurrence of failures is represented by discontinuous steps in the function $\chi_i(t)$, transitioning between 1 and 0, and vice versa. If a heating source experiences a failure, a step from 1 to 0 is observed, indicating a cessation of heat generation. Conversely, a step from 0 to 1 signifies the successful restart of a previously failed source.

The following section provides a comprehensive overview of the proposed approach and formulation of the inverse problem, building upon our recent research [19]. This presentation aims to delve into the details of the approach, highlighting its key aspects and addressing the specific challenges associated with solving the inverse problem.

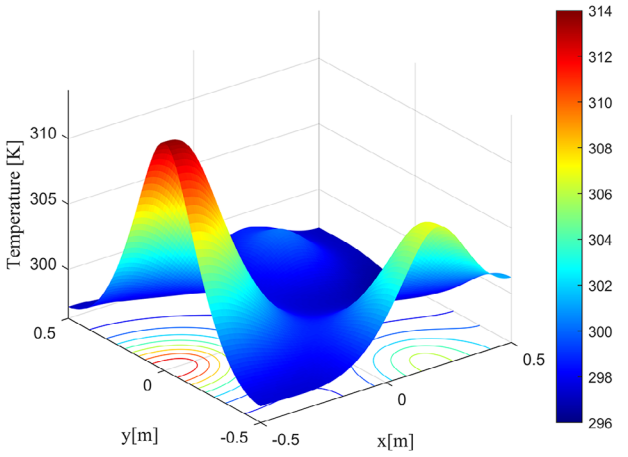

(a) Results of the Direct Problem in 2D Geometry with 3D Visualization

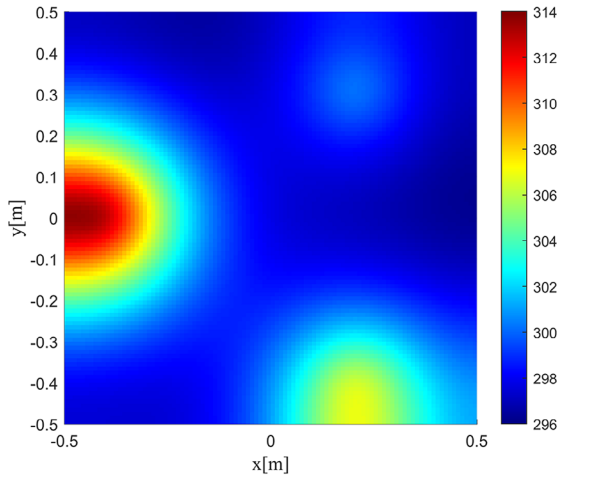

(b) Results of the Direct Problem in 2D Geometry with 2D Visualization

FIGURE 3 Solving the direct problem using finite elements method: Temperature distribution at t = 3600 s under normal operating conditions (no failures).

3 | APPROACH 1: THE CONJUGATE GRADIENT METHOD

3.1 | The inverse problem

In order to determine the switching times for the heating sources, it is necessary to express the function $\chi_i(t)$ in a continuous form. To achieve this, let us consider that the source i has experienced a total of n_i failures. In this case, the continuous representation of $\chi_i(t)$ can be given by the following function:

$$\chi_i(t) = 1 - \frac{1}{\pi}\sum_{j=1}^{n_i}\left(\operatorname{atan}\left(\frac{t - t^i_{nok,j}}{\eta}\right) - \operatorname{atan}\left(\frac{t - t^i_{ok,j}}{\eta}\right)\right). \tag{6}$$

Here, $t^i_{nok,j}$ represents the time instants when source i fails (i.e. when $\chi_i(t)$ transitions from 1 to 0, also known as the falling edge), while $t^i_{ok,j}$ represents the time instants when $\chi_i(t)$ transitions from 0 to 1 (rising edge). The impact of the regularization parameter η is demonstrated in Figure 4.

For each heating source $i = 1, \ldots, n_{\text{heat}}$, it is necessary to identify the switching times $t^i_{nok,j}$ and $t^i_{ok,j}$, where j ranges from 1 to n_i, representing the number of failures and restarts for each source. An example demonstrating the behavior of the function $\chi_i(t)$ $i = 1, 2, 3$ is depicted in Figure 4. In this example, source 1 experiences a failure at 1000s and restarts operation at 2500s, source 2 fails at 2000s, and source 3 operates without any failure. In the subsequent analysis, it is assumed that the number of failures n_i for each source is already known. However, if this information is not available initially, it presents an additional challenge. Nonetheless, this challenge can be overcome by adapting the method described below. The parameter vector that contains unknown parameters is denoted as:

$$\boldsymbol{\tau} = [\boldsymbol{\tau}^1, \ldots, \boldsymbol{\tau}^{n_{\text{heat}}}], \tag{7}$$

where each component $\boldsymbol{\tau}^i$ is defined as:

$$\boldsymbol{\tau}^i = \left[t^i_{\text{nok},1}, t^i_{\text{ok},1}, \ldots, t^i_{\text{nok},n_i}, t^i_{\text{ok},n_i}\right]. \tag{8}$$

The total number of unidentified parameters is given by $N = \sum_{i=1}^{n_{\text{heat}}}\left(\sum_{j=1}^{n_i} 2n_j\right)$: $\boldsymbol{\tau} = \left(\tau^i_j\right)_{\substack{i=1,\ldots,n_{\text{heat}} \\ j=1,\ldots,2n_i}}$. The odd-indexed components of $\boldsymbol{\tau}$ correspond to failure times, while the even-indexed components correspond to restart times.

To achieve the parametric identification, a technique based on minimizing the output error is employed. The goal is to adjust the undetermined parameters $\boldsymbol{\tau}$ such that the data predicted by the mathematical model aligns with the observed data. This is accomplished by employing a quadratic criterion, given by:

$$J(\boldsymbol{\tau}) = \frac{1}{2}\sum_{i=1}^{4}\int_0^{t_f}\left(T(C_i, t, \boldsymbol{\tau}) - \hat{T}_i(t)\right)^2 dt, \tag{9}$$

where $T(C_i, t, \boldsymbol{\tau})$ represents the predicted data from the mathematical model at the sensor C_i and $\hat{T}_i(t)$ denotes the corresponding observed data. The criterion $J(\boldsymbol{\tau})$ quantifies the discrepancy between the model predictions and the actual observations, with the aim of minimizing this discrepancy through parameter adjustments. IHCP can be formulated as follows:

- Given: a complete set of input parameters $\{e, t_f, \rho C, \lambda, \Phi, h, T_0\}$
- Objective: find the unknown $\boldsymbol{\tau}^*$ such that the quadratic criterion (9) is minimal:

$$\boldsymbol{\tau}^* = \operatorname*{Arg\,min}_{\boldsymbol{\tau}} J(\boldsymbol{\tau}),$$

subject to the constraint: $T(x, y, t)$ is the solution of the direct problem (1).

IHCPs are considered ill-posed problems due to their sensitivity to small perturbations in measurements, which can lead to significant errors in parameter estimation. Therefore, it is essential to employ an appropriate method that can mitigate these issues. One such method is the Conjugate Gradient Iterative Regularization Method (CGM) [38]. This iterative algorithm

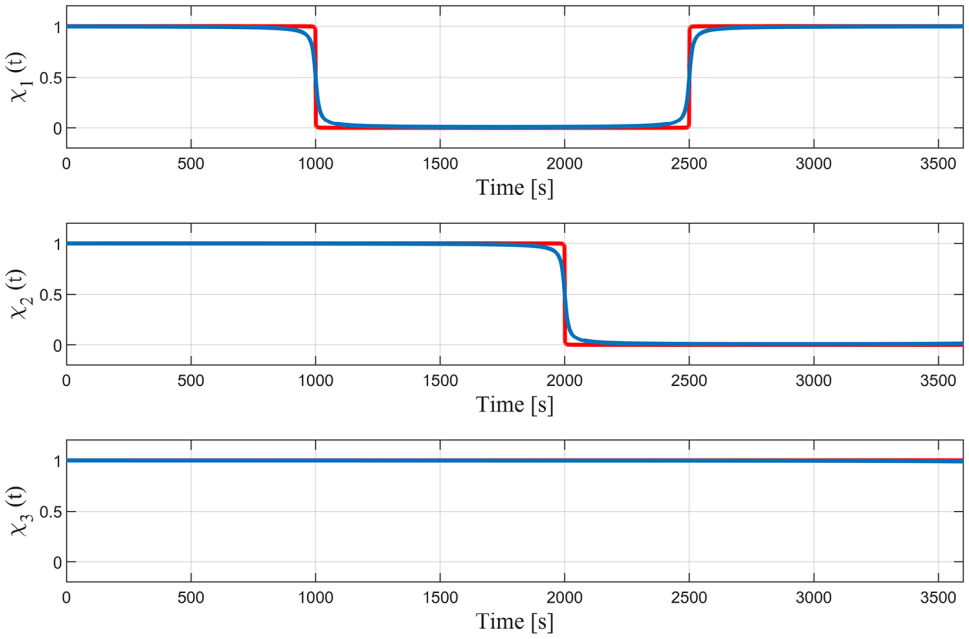

FIGURE 4 Illustrations of failures $\chi_1(t)$, $\chi_2(t)$ and $\chi_3(t)$ are provided, with the blue curve representing $\eta = 10$ and the red curve representing $\eta = 0.1$..

is based on the solution of three well-posed problems in each iteration (k):

- Solve the direct problem (1) to calculate the criterion (9).
- Solve the adjoint problem to obtain an accurate estimation of the gradient of the criterion.
- Solve the sensitivity problem to determine the descent step size in the direction of descent.

3.2 | The sensitivity problem

The variations in the unknown parameters are given by: $\boldsymbol{\tau}^+ = \boldsymbol{\tau} + \varepsilon\delta\boldsymbol{\tau}$. Consequently, the resulting variations in $\chi_i(t)$ are expressed as:

$$\chi_i^+(t) = \chi_i(t) + \sum_{j=1}^{2n_i}\left(\varepsilon\delta\boldsymbol{\tau}^i{}_j \frac{\mathrm{d}\,\chi_i}{\mathrm{d}\,\boldsymbol{\tau}^i_j}\right),$$
$$= \chi_i(t) + \varepsilon\sum_{j=1}^{2n_i}\left(\delta\boldsymbol{\tau}^i{}_j \frac{1}{\pi}\frac{\eta(-1)^{j+1}}{\eta^2 + \left(t - \boldsymbol{\tau}^i_j\right)^2}\right).$$

The varied temperature $T^+(x,y,t)$ then satisfies the following equations:

$$\begin{cases} \rho C\dfrac{\partial T^+(x,y,t)}{\partial t} - \lambda\Delta T^+(x,y,t) = \dfrac{\Phi - 2h\left(T^+(x,y,t) - T_0\right)}{e}, \\ T^+(x,y,0) = T_0, \quad (x,y)\in\Omega, \\ -\lambda\dfrac{\partial T^+(x,y,t)}{\partial\vec{n}} = 0, \quad (x,y,t)\in\Gamma\times\left[0,t_f\right]. \end{cases} \tag{10}$$

By comparing equations (10) with equations (1), the following equations are obtained:

$$\begin{cases} \rho C\dfrac{\partial(T^+ - T)}{\partial t} - \lambda\Delta(T^+ - T) = \\ \qquad\qquad \dfrac{\left(\sum_{i=1}^{n_{heat}} f_i g_i\left(\chi_i^+ - \chi_i\right)\right) - 2h(T^+ - T)}{e}, \\ T^+(x,y,0) - T(x,y,0) = 0, \quad (x,y)\in\Omega, \\ -\lambda\dfrac{\partial T^+(x,y,t)}{\partial\vec{n}} + \lambda\dfrac{\partial T(x,y,t)}{\partial\vec{n}} = 0, \quad (x,y,t)\in\Gamma\times\left[0,t_f\right]. \end{cases} \tag{11}$$

Taking into account that $T^+ = T + \varepsilon\delta T$, as $\varepsilon\to 0$, equations (11) can be simplified as follows:

$$\begin{cases} \rho C\dfrac{\partial\delta T}{\partial t} - \lambda\Delta\delta T = \\ \qquad\qquad \dfrac{\left(\sum_{i=1}^{n_{heat}}\left(\dfrac{f_i g_i\eta}{\pi}\sum_{j=1}^{2n_i}\left(\dfrac{(-1)^{j+1}\delta\boldsymbol{\tau}^i_j}{\eta^2 + \left(t - \boldsymbol{\tau}^i_j\right)^2}\right)\right)\right) - 2h\delta T}{e}, \\ \delta T(x,y,0) = 0, \quad (x,y)\in\Omega, \\ -\lambda\dfrac{\partial\delta T(x,y,t)}{\partial\vec{n}} = 0, \quad (x,y,t)\in\Gamma\times[0,t_f]. \end{cases} \tag{12}$$

During each iteration, the descent depth is determined to minimize the criterion along the descent direction $\boldsymbol{d}^{k+1}$:

$$\gamma^{k+1} = \underset{\gamma^k \in \mathbb{R}^2}{\arg\min}\, J\left(\boldsymbol{\tau}^k - \gamma d^{k+1}\right) = \frac{\sum_{i=1}^{4} \int_0^{t_f} \left(T\left(C_i, t; \boldsymbol{\tau}^k\right) - \hat{T}_i(t)\right) \delta T\left(C_i, t, \boldsymbol{\tau}^k\right) dt}{\sum_{i=1}^{4} \int_0^{t_f} \left(\delta T\left(C_i, t, \boldsymbol{\tau}^k\right)\right)^2 dt}. \tag{13}$$

3.3 | The adjoint problem

The purpose of this problem is to determine the gradient of the cost-function: $\nabla J^k = \left(\frac{\partial J^k}{\partial \tau_j^i}\right)_{\substack{i=1,\dots,n_{\text{heat}} \\ j=1,\dots,2n_i}}$. In order to accomplish this, we present the Lagrangian multipliers $\psi(x, y, t)$ and the Lagrangian:

$$\mathfrak{L}(T, \boldsymbol{\tau}, \psi) = J(\boldsymbol{\tau}) + \iint_{\Omega \times [0, t_f]} \left(\rho C \frac{\partial T}{\partial t} - \lambda \Delta T - \frac{\Phi - 2h(T - T_0)}{e}\right) \psi \, d\Omega \, dt. \tag{14}$$

The variation of the Lagrangian is:

$$\delta \mathfrak{L}(T, \boldsymbol{\tau}, \psi) = \frac{\partial \mathfrak{L}}{\partial T} \delta T + \sum_{i=1}^{n_{\text{heat}}} \left(\sum_{j=1}^{2n_i} \left(\frac{\partial \mathfrak{L}}{\partial \tau_j^i} \delta \tau_j^i\right)\right) + \frac{\partial \mathfrak{L}}{\partial \psi} \delta \psi. \tag{15}$$

The Lagrange multiplier ψ is fixed in order to satisfy following equation: $\frac{\partial \mathfrak{L}}{\partial T} \delta T = 0$. In addition, since the temperature T is a solution of (1), then $\delta J(\boldsymbol{\tau}) = \delta \mathfrak{L}(T, \boldsymbol{\tau}, \psi)$. In order to determine $\psi(x, y, t)$, it is necessary to develop the Equation (15) from (14). The latter includes several terms:

$$\frac{\partial \mathfrak{L}}{\partial T} \delta T = \iint_{\Omega \times [0, t_f]} \left(\sum_{i=1}^{4} \left(T(C_i, t) - \hat{T}_i(t)\right) \delta T D_i\right) d\Omega \, dt + \rho C \iint_{\Omega \times [0, t_f]} \frac{\partial \delta T}{\partial t} \psi \, d\Omega \, dt + \iint_{\Omega \times [0, t_f]} \left(-\lambda \Delta \delta T + \frac{2h}{e} \delta T\right) \psi \, d\Omega \, dt. \tag{16}$$

In Equation (16), the term D_i represents the Dirac distribution at the sensor C_i. Thus, we can decompose (15) as follows:

$$\delta \mathfrak{L}(T, \boldsymbol{\tau}, \psi) = \iint_{\Omega \times [0, t_f]} E \; dxdydt + \rho C \, \delta \mathfrak{L}_1 + \delta \mathfrak{L}_2 + \sum_{i=1}^{n_{\text{heat}}} \left(\sum_{j=1}^{2n_i} \left(\frac{\partial \mathfrak{L}}{\partial \tau_j^i} \delta \tau_j^i\right)\right). \tag{17}$$

where:

$$E(x, y, t) = \sum_{i=1}^{4} \left(T(C_i, t) - \hat{T}_i(t)\right) \delta T D_i.$$

$$\delta \mathfrak{L}_1(x, y, t) = \iint_{\Omega \times [0, t_f]} \frac{\partial \delta T(x, y, t)}{\partial t} \psi(x, y, t) \; dxdydt.$$

$$\delta \mathfrak{L}_2(x, y, t) = \iint_{\Omega \times [0, t_f]} \left(-\lambda \Delta \delta T(x, y, t) + \frac{2h}{e} \delta T(x, y, t)\right) \times \psi dxdydt.$$

Several integrations by parts, the use of Green's theorem as well as the formulation of the sensitivity problem allow to simplify:

$$\delta \mathfrak{L}_1 = \int_{\Omega} \delta T(x, y, t_f) \psi(x, y, t_f) \; dxdy - \iint_{\Gamma \times [0, t_f]} \delta T \frac{\partial \psi}{\partial t} \; dxdydt.$$

$$\delta \mathfrak{L}_2 = - \iint_{\Omega \times [0, t_f]} \lambda \Delta(\psi) \delta T \; dxdydt + \iint_{\Gamma \times [0, t_f]} \lambda \delta T \frac{\partial \psi}{\partial \vec{n}} \; dxdydt \iint_{\Omega \times [0, t_f]} \frac{2h}{e} \delta T \psi \; dxdydt.$$

As ψ is fixed so that $\frac{\partial \mathfrak{L}}{\partial T} \delta T = 0$, then ψ is solution of the following system (adjoint problem):

$$\begin{cases} \rho C \dfrac{\partial \psi(x, y, t)}{\partial t} + \lambda \Delta \psi(x, y, t) = E(x, y, t) + \dfrac{2h}{e} \psi(x, y, t), \\ \psi(x, y, t_f) = 0, \qquad (x, y) \in \Omega \\ \dfrac{\partial \psi(x, y, t)}{\partial \vec{n}} = 0, \qquad (x, y, t) \in \Gamma \times \left[0, t_f\right]. \end{cases} \tag{18}$$

If ψ is a solution of the adjoint problem described by the PDEs (18) while T is a solution of the direct problem described by the PDEs (1), Equation (15) becomes:

$$\delta \mathfrak{L}(T, \boldsymbol{\tau}, \psi) = \sum_{i=1}^{n_{\text{heat}}} \left(\sum_{j=1}^{2n_i} \left(\frac{\partial \mathfrak{L}}{\partial \tau_j^i} \delta \tau_j^i\right)\right).$$

In addition, as $\delta J(\boldsymbol{\tau}) = \delta \mathfrak{L}(T, \boldsymbol{\tau}, \psi)$ and:

$$\frac{\partial \mathfrak{L}}{\partial \tau_j^i} \delta \tau_j^i = \iint_{\Omega \times [0, t_f]} \left(\frac{f_i g_i \eta}{\pi e} \left(\frac{(-1)^j \delta \tau_j^i}{\eta^2 + \left(t - \tau_j^i\right)^2}\right)\right) \psi \; dxdydt, \tag{19}$$

ALGORITHM 1 CGM algorithm.

i. Choose an initialization $\boldsymbol{\tau}^k$ for the iteration $k = 0$ for the switching instants (failures and restarts).

ii. Solve the direct problem (1) to estimate the temperature T^k and estimate the criterion $J\left(\boldsymbol{\tau}^k\right)$ according to (9).

iii. Resolution of the adjoint problem (18) to calculate the gradient $\overrightarrow{\nabla J^k} = \left(\frac{\partial J^k}{\partial \tau_j^i}\right)_{\substack{i=1,\ldots,n_{\text{heat}} \\ j=1,\ldots,2n_i}}$ according to (20). Deduce the descent direction:

$$\boldsymbol{d}^{k+1} = -\overrightarrow{\nabla J^k} + \beta_k \boldsymbol{d}^k, \quad \text{with:} \quad \beta_k = \frac{\left\|\overrightarrow{\nabla J^k}\right\|^2}{\left\|\overrightarrow{\nabla J^{k-1}}\right\|^2},$$

(except at iteration $k = 0$ for which $\beta_0 = 0$).

iv. Solving the sensitivity problem (12) to calculate the sensitivity functions δT^k and deducing the descent depth γ^{k+1} according to (13).

v. Determination of the new estimator for the switching times: $\boldsymbol{\tau}^{k+1} = \boldsymbol{\tau}^k - \gamma^{k+1}\boldsymbol{d}^{k+1}$ then returning to step (ii).

the expression of the gradient is then:

$$\frac{\partial J}{\partial \boldsymbol{\tau}_j^i} = \iint_{\Omega\times[0,t_f]} \left(\frac{f_i g_i \eta}{\pi e} \left(\frac{(-1)^j}{\eta^2 + \left(t - \boldsymbol{\tau}_j^i\right)^2} \right) \right) \psi \, dxdydt. \quad (20)$$

3.4 | Algorithm

The conjugate gradient iterative regularization method is implemented in Algorithm 1. The algorithm stopped in step (ii) when the criterion is deemed sufficiently small. The stopping criterion is chosen according to the measurement noise on the observations $\hat{T}_i(t)$, temperatures measured at the sensors C_i. The whole identification method has been successfully implemented in [39–41].

3.5 | Example

Considering the illustrative context where the identification of the failure of source 1 has to be performed from the observations obtained in Figure 5. In this section, the measurements collected from the four sensors data are treated with an uncertainty characterized by zero-mean Gaussian noise and distinct standard deviations σ. In Figure 5, it is a standard deviation $\sigma = 0.5°C$. In order to implement the CGM algorithm, a J_{stop} threshold must be defined. The stopping criterion to stop the iterative minimization of the criterion is chosen according to the criterion proposed by [33, 42]:

$$J_{\text{stop}} = \Delta t \; N_c \; N_t \; \sigma^2, \quad (21)$$

where $N_c = 4$ is the number of sensors, $N_t = 400$ is the number of measurements per sensor, $\Delta t = 9$ s is the time sampling

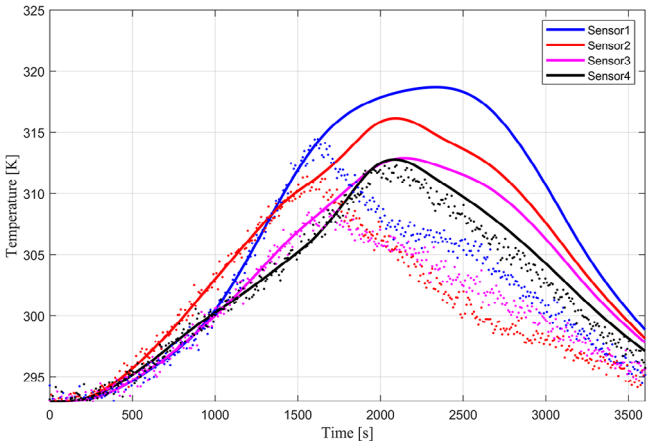

FIGURE 5 Sensor measurements: case when the heat source Φ_1 fail with noise $\sigma = 0.5°C$, represented as discrete points, without any failure and noise, represented as continuous data.

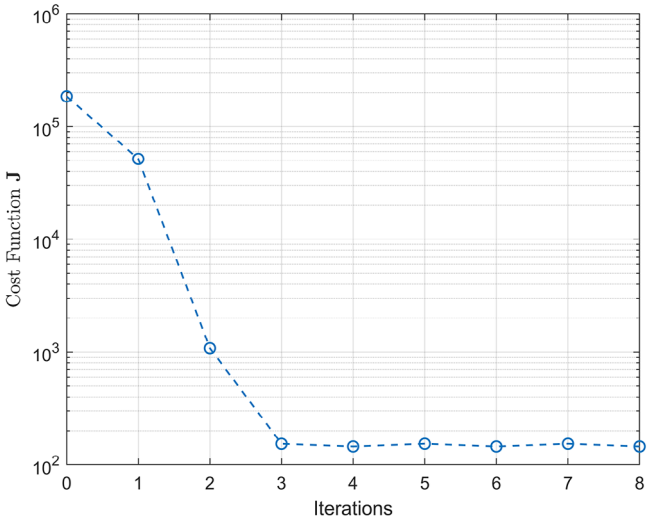

FIGURE 6 Example of Criterion evolution in case $\sigma = 0.5°C$.

step between each measurement and σ^2 is the variance of the Gaussian measurement noise. On a personal computer with the following characteristics, numerical results are achieved using the Comsol-Multiphysics solver interfaced with Matlab software: CPU: Intel® Core(TM) i5-10210U CPU 2.11 GHz, RAM: 8.00 Go, OS: Windows 10 (64).

In the following, we consider the results obtained with an initialization of the failure time of $t^1_{\text{nok},1} = 500$ s. For example, Figure 6 shows the cost function versus iteration number. With a stop-criterion (21), the identification converged in a single simulation in 10 min. The following Table 2 shows the results of the identification process for different noise levels. On 30 simulations, the results are presented as the mean and standard deviation (in brackets). The last row of the previous table corresponds to the identification of the failure times for the data in Figure 5, with CGM algorithm (based on the iterative resolution of three well-posed problems). When the noise levels of the sensors are less significant, this approach gives a satisfying result

TABLE 2 Heat source Φ_1 failure times with various noise levels.

	J_{stop}	Instant $t^1_{\text{nok},1}$
$\sigma = 0.1°C$	144	1500.13s (2.29)
$\sigma = 0.5°C$	3600	1498s (3.81)
$\sigma = 1°C$	14400	1497.15s (6.10)

to the identification of the failure times for the first source. Once the measurement noise of the sensors become more important, the CGM still gives an excellent result with superior accuracy.

Following the presentation and analysis of the first approach, it is essential to emphasize its significance. In the subsequent section, we introduce a second method based on the Bayesian filter, which builds upon our recent work [34]. This alternative approach serves to further enhance our understanding and broaden the scope of our investigation.

4 | APPROACH 2: THE BAYESIAN FILTER

4.1 | State estimation problem

State estimation inverse problems [24, 43, 44] are one of the most interests in countless practical applications, described as evolution and observation models. In these types of problems, measurable data and prior knowledge about physical phenomena are employed sequentially to estimate the necessary dynamic variables and solved by the Bayesian filters [24, 43]. The Kalman filter is the most commonly used Bayesian filter technique, especially with linear systems with additive Gaussian noises.

In this context, and in order to define the evolution and observation problems, we need to rewrite the direct problem (1) as an state estimation problem. For this purpose, a numerical approach based on the finite difference method is considered [45]. The discretization of the system (1) using finite differences and the construction of the evolution and observation models are explicitly demonstrated and analyzed in [34]. Consequently, the application can be formulated as follows:

$$\begin{cases} \boldsymbol{T}^{k+1} = \boldsymbol{L}\cdot\boldsymbol{T}^{k} + \boldsymbol{M}\cdot\boldsymbol{G}^{k} + \boldsymbol{H}, \\ \boldsymbol{T}^{k}_{\boldsymbol{obs}} = \boldsymbol{P}\cdot\boldsymbol{T}^{k}, \end{cases} \tag{22}$$

where $\boldsymbol{T}^{k}$ is a matrix containing temperature of all discretised points of the plate at the instant k, $\boldsymbol{L}$ is the transition matrix, encodes the linear combination of $\boldsymbol{T}^{k}$, that connects state k to state $k+1$, the matrix $\boldsymbol{M}$ encodes the coordinates of the Gaussian distribution surrounding the point (x_i, y_i) based on the fixed source's spatial support f_i^k. The heat flux g_i^k $i = 1, \dots, 3$, is encoded by the matrix $\boldsymbol{G}^{k}$, and the position of the fixed sensors is encoded by the matrix $\boldsymbol{C}$. Finally, $\boldsymbol{H}$ is a constant vector that depends on discretization and model parameters.

4.2 | The inverse problem

The inverse problem, considered in this application, consists in extracting information from the state vectors from the observed measurements. This formulation of the inverse problem is done in a Bayesian framework using the Kalman filter. The Kalman filter was used, with the assumption that both the evolution and observation models (22) are linear. The noises are assumed to be Gaussian with known means and covariances, and to be additive in such models. The system (22) is then modified as follows:

$$\begin{cases} \boldsymbol{T}^{k+1} = \boldsymbol{L}\cdot\boldsymbol{T}^{k} + \boldsymbol{M}\cdot\boldsymbol{G}^{k} + \boldsymbol{H} + \boldsymbol{w}_k, \\ \boldsymbol{T}^{k}_{obs} = \boldsymbol{P}\cdot\boldsymbol{T}^{k} + \boldsymbol{v}_k, \end{cases} \tag{23}$$

where $\boldsymbol{w}_k$, $\boldsymbol{v}_k$ are the evolution and observation noises, respectively, with zero means and covariances matrices $\boldsymbol{Q}$ and $\boldsymbol{R}$, respectively. To estimate the input vector $\boldsymbol{G}^{k}$, a technique involves modifying the classical Kalman filter to incorporate the input vector into the state vector. By including the input vector, we can estimate the behavior of the heat flux g_i^k for each source $(i = 1, \dots, 3)$. This estimation of the heat flux behavior provides valuable insights can be used to identify potential heat source failures. Following the same methodology described in [34], the new modified system can be represented as follows:

$$\begin{cases} \boldsymbol{\Theta}^{k+1} = \boldsymbol{L}'\cdot\boldsymbol{\Theta}^{k} + \boldsymbol{H}' + \boldsymbol{w}'_{\boldsymbol{k}}, \\ \boldsymbol{T}^{k}_{obs} = \boldsymbol{P}'\cdot\boldsymbol{\Theta}^{k} + \boldsymbol{v}_{\boldsymbol{k}}, \end{cases} \tag{24}$$

where:

$$\boldsymbol{\Theta}^{k+1} = \begin{bmatrix} \boldsymbol{T}^{k+1} \\ \boldsymbol{G}^{k+1} \end{bmatrix}, \quad \boldsymbol{L}' = \begin{bmatrix} \boldsymbol{L} & \boldsymbol{M} \\ \boldsymbol{0} & \mathbf{I} \end{bmatrix} \quad \text{and} \quad \boldsymbol{P}' = \begin{bmatrix} \boldsymbol{P} & 0 \end{bmatrix}.$$

Finally, after reformulating the system (23) into (24) with the integration of the input vector $\boldsymbol{G}$ into the state vector, we are ready to use the Kalman filter. The posteriori density is Gaussian and the Kalman filter gives the optimal solution to the state estimation problem. $\boldsymbol{L}'$ and $\boldsymbol{P}'$ are given matrices for the corresponding state $\boldsymbol{\Theta}^{k}$ and observation $\boldsymbol{T}^{k}_{obs}$, also, $\boldsymbol{H}'$ is a constant vector for the model of the state evolution $\boldsymbol{\Theta}^{k}$. In the following, $\boldsymbol{\Theta}$ is a Gaussian with calculable mean and covariance. We denote by $\boldsymbol{\mu}$ and $\boldsymbol{\Sigma}$ the means and covariance, respectively. Given that $\boldsymbol{Q}$ and $\boldsymbol{R}$ are also Gaussian, Considering the noises, $\boldsymbol{w}'$ with zero mean multivariate normal distribution $\mathcal{N}$ and covariance matrix $\boldsymbol{Q}$: $\boldsymbol{w}' \sim \mathcal{N}(0, \boldsymbol{Q})$, and $\boldsymbol{v}$ with a zero mean and covariance matrix $\boldsymbol{R}$: $\boldsymbol{v} \sim \mathcal{N}(0, \boldsymbol{R})$. The prediction and update steps of the Kalman filter, for each $k = 1, \dots, t^*$, where $t^* = t_f/\Delta t_{obs}$, are given by Algorithm 2.

In the algorithm presented, the Kalman gain matrix is denoted as $\boldsymbol{K}_k$, while $\boldsymbol{T}^{k}_{obs}$ represents the observation vector at time k. It is important to note that in the research paper, temperature measurements are not taken continuously but rather at

ALGORITHM 2 Kalman filter.

i. Initialize: $\hat{\boldsymbol{\mu}}_{0|0}$ and $\boldsymbol{\Sigma}_{0|0}$.

ii. For $k = 1, 2, \ldots, t^*$:

Prediction:

$$\hat{\boldsymbol{\mu}}_{k|k-1} = \boldsymbol{L}'\hat{\boldsymbol{\mu}}_{k-1|k-1} + \boldsymbol{H}', \tag{25}$$

$$\hat{\boldsymbol{\Sigma}}_{k|k-1} = \boldsymbol{L}'\hat{\boldsymbol{\Sigma}}_{k-1|k-1}\boldsymbol{L}'^{T} + \boldsymbol{Q}. \tag{26}$$

Update:

$$\boldsymbol{K}_k = \hat{\boldsymbol{\Sigma}}_{k|k-1}\boldsymbol{P}'^{T}\left(\boldsymbol{P}'\hat{\boldsymbol{\Sigma}}_{k|k-1}\boldsymbol{P}'^{T} + \boldsymbol{R}\right)^{-1}, \tag{27}$$

$$\hat{\boldsymbol{\mu}}_{k|k} = \hat{\boldsymbol{\mu}}_{k|k-1} + \boldsymbol{K}_k\left(\boldsymbol{T}^{k}_{obs} - \boldsymbol{P}'\hat{\boldsymbol{\mu}}_{k|k-1}\right), \tag{28}$$

$$\hat{\boldsymbol{\Sigma}}_{k|k} = \left(\mathbf{I} - \boldsymbol{K}_k\boldsymbol{P}'\right)\hat{\boldsymbol{\Sigma}}_{k|k-1}. \tag{29}$$

9-s intervals. Consequently, if there is no measurement available at time k, then $\hat{\boldsymbol{\mu}}_{k|k} = \hat{\boldsymbol{\mu}}_{k|k-1}$.

Furthermore, for the purpose of determining the failure and restart times of the heat sources, an offline analysis of this application is assumed in the research paper. This offline analysis facilitates the identification of the distinct instants when the sources experience failures and restarts. In this scenario, the Kalman smoother [46] likewise known as Rauch-Tung-Striebel (RTS) smoother [47] could provide a more accurate estimate of the state vector. The Kalman smoother offers an efficient method for computing the mean and covariance matrix, circumventing the need to invert large matrices. It utilizes available information more comprehensively than filtering, resulting in enhanced outcomes. Essentially, the Kalman smoother builds upon the outputs of the Kalman filter, which incorporates all available measurements - future, present, and past - and processes this data in a reverse chronological order [48, 49]. Figure 7 provides a detailed illustration of both the Kalman filtering and smoothing processes. For this algorithm, we assume that the Kalman filter has already been applied; the reverse steps are detailed in (Algorithms 3 and 4).

4.3 | Estimation methodology

To estimate the failure restart times, an assumption was made that the failures of the sources are independent events, allowing them to be treated individually. Furthermore, the knowledge of the theoretical signal of each source without failure, denoted as g_i^k and graphically represented in Figure 2, was utilized. Given a set of candidate vectors χ_{cand}, the problem is to find the optimal candidate vector χ_{opt} that minimizes the squared error (SE) between $g_i^k \times \chi^i_{cand}$ and $\widehat{g}_i^k$. To have a better understanding of this search approach, we refer readers to our previous work [34]. Mathematically, this can be expressed as follows:

$$\chi^i_{\text{opt}} = \underset{\chi_{cand}}{\text{Arg min}} \sum_{k}^{t^*} \left(g_i^k \times \chi^i_{cand} - \widehat{g}_i^k\right)^2. \tag{30}$$

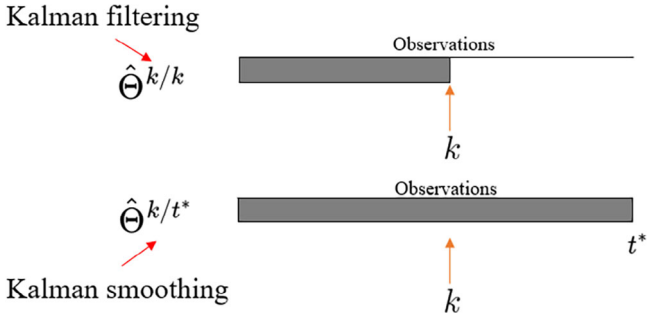

FIGURE 7 Description of filtering and smoothing processes.

ALGORITHM 3 Kalman Smoother.

i. Initialize: $\hat{\boldsymbol{\mu}}_{t^*|t^*}, \hat{\boldsymbol{\Sigma}}_{t^*|t^*}$.

ii. For $k = t^* - 1, t^* - 2, \ldots, 1$:

$$\boldsymbol{\mathcal{P}}_k = \hat{\boldsymbol{\Sigma}}_{k|k}\boldsymbol{L}'^{T}\hat{\boldsymbol{\Sigma}}^{-1}_{k+1|k}.$$

$$\hat{\boldsymbol{\mu}}_{k|t^*} = \hat{\boldsymbol{\mu}}_{k|k} + \boldsymbol{\mathcal{P}}_k(\boldsymbol{\mu}_{k+1|t^*} - \hat{\boldsymbol{\mu}}_{k+1|k}).$$

$$\hat{\boldsymbol{\Sigma}}_{k|t^*} = \hat{\boldsymbol{\Sigma}}_{k|k} + \boldsymbol{\mathcal{P}}_k(\boldsymbol{\Sigma}_{k+1|t^*} - \hat{\boldsymbol{\Sigma}}_{k+1|k})\boldsymbol{\mathcal{P}}_k^{T}.$$

ALGORITHM 4 Search strategy algorithm.

i. Initialize and define the bounds of the candidate vector χ^i_{cand}.

ii. Compute the squared error (SE) between $g_i(t) \times \chi^i_{cand}$ and $\widehat{g}_i(t)$.

iii. Solve problem (30) by performing an iterative search to find the value of χ^i_{cand} that minimizes the squared error, while respecting the constraints defined by the bounds.

iv. Return the optimal value of χ^i_{opt} that minimizes the squared error, along with the minimum value of the squared error.

After presenting the methodology in detail, we are now ready to demonstrate its effectiveness through a performance result.

4.4 | Example

For the purpose of demonstrating the proposed methodology, let us consider the previous illustrative context where the first source has a failure time $t = 1500$s. Parameters are given in the following Table 3 and the evolution of the temperatures at the four sensors C_1, C_2, C_3, C_4 are shown in Figure 5, similar to the previous section 3.5, the measurement data are treated with an uncertainty characterized by zero-mean Gaussian noise and distinct standard deviations σ.

To illustrate the effect of such parameters, the mean and standard deviation (in brackets) of 30 simulations are provided for each configuration. The results are given in Table 4 with different noise levels, and they are obtained after 65,66 s in a single simulation, for a total of 36 min registered after 30 simulations. With this approach, it is clear that the search strategy gives a good result for estimating the failure times, when the noise levels of the sensors are less significant. However, the

TABLE 3 Mathematical model parameters.

Symbol	Definition	Values
ρc	Volumetric heat	$2.421.10^6$ J · m^{-3} · K^{-1}
h	Natural convection coefficient	10 W · m^{-2}K^{-1}
λ	Thermal conductivity	178 W · m^{-1} · K^{-1}
θ_0	Initial temperature	293 K
t_f	Final time	3600 s
e	Thickness	$2 \cdot 10^{-3}$ m
Δt	Time step	3 s
Δt_{obs}	Time step of the observations	9 s
$\Delta x, \Delta y$	Space step	0.05m

TABLE 4 Failure times for different noise levels.

	Failure $t^1_{\text{fail},1}$
$\sigma = 0.1°$C	1500s (1.03)
$\sigma = 0.5°$C	1516s (3.09)
$\sigma = 1°$C	1531.5s (6.19)

accuracy of the failure time detection is reduced considerably due to the increase in the measurement noise of the sensors, while taking into account the number of sensors used for this particular application.

In the following section, we explore different configurations to present the implementation of the Conjugate Gradient Method (CGM) and compare it to the second approach based on Kalman smoother (KS). Through this in-depth evaluation, we aim to provide a comprehensive assessment that highlights both the advantages and disadvantages of our recent approach.

5 | NUMERICAL RESULTS

In this section, we simulate several scenarios to demonstrate the effectiveness of our proposed methodologies. To avoid the inverse crime, data were gathered from a Comsol-Multiphysics simulation, employing different parameters: a time step of $\Delta t = 1$s and a spatial step of $\Delta x = \Delta y = 0.01$m. This data was then analyzed using Matlab. To realistically replicate the uncertainties in sensor data, as commonly experienced in real-world systems, we introduced Gaussian noise with a zero mean to the sensor data. This noise varied in standard deviations σ, simulating different levels of measurement uncertainty. Specifically, we explored three levels of noise: $\sigma = 0.1°$C, $\sigma = 0.5°$ and $\sigma = 1°$C.These values were selected to mirror the range of uncertainties typically found in sensor measurements in such thermal systems.

To comprehensively evaluate the impact of these differing levels of uncertainty, we conducted a Monte Carlo simulation for each noise configuration. The outcomes of these simulations are depicted in terms of mean and standard deviation, derived from 30 simulations for each scenario. This methodology offers

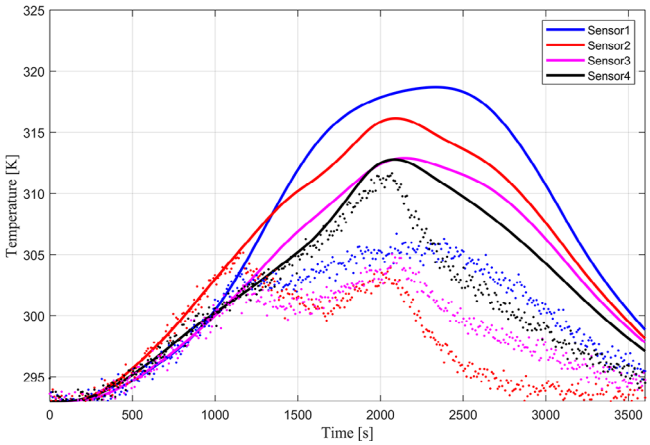

FIGURE 8 Sensor measurements: case when the heat sources Φ_1 and Φ_2 fails, represented as discrete points, without any failure and noise, represented as continuous data.

TABLE 5 Heat sources Φ_1 and Φ_2 failure times identification with varying noise levels.

		Instant $t^1_{\text{nok},1}$	Instant $t^2_{\text{nok},1}$
$\sigma = 0.1°$C	CGM	997s (1.95)	1997s (2.54)
	KS	1001s (2.17)	2003s (2.31)
$\sigma = 0.5°$C	CGM	998.76s (4.40)	1997.4s (4.60)
	KS	1003.2s (5.06)	2008.9s (4.41)
$\sigma = 1°$C	CGM	996s (11.73)	2000.7s (13.37)
	KS	975.8s (9.21)	2041.7s (7.68)

a detailed insight into how varying degrees of sensor noise affect the precision and reliability of our failure identification process across diverse scenarios.

5.1 | Source separation

After having successfully identified the failure instants for a single source by both approaches, the objective in this new scenario is to identify the failure instants for two distinct sources. In this configuration, we consider that first source fails at $t^1_{\text{nok},1} = 1000$ s and the second source fails at $t^2_{\text{nok},1} = 2000$ s. For example, the measurements at the four sensors are given in Figure 8 with standard deviation $\sigma = 0.5°$. Using the same parameters in Table 3, we obtain the results presented in Table 5, starting with the initialization $t^1_{\text{nok},1} = 500$ s and $t^2_{\text{nok},1} = 1000$ s. Finally, We denote the results given by the first approach as (CGM) and the second approach as (KS), respectively. In Figure 9, an example representing the probability density function (PDF) for both approaches when the first source fails, based on a sample of 30 simulations. The PDF result is obtained by using the normal distribution.

In Table 5, it is evident that the two approaches have successfully identified the failure instants for two separate sources. When the measurement noises are less significant, both

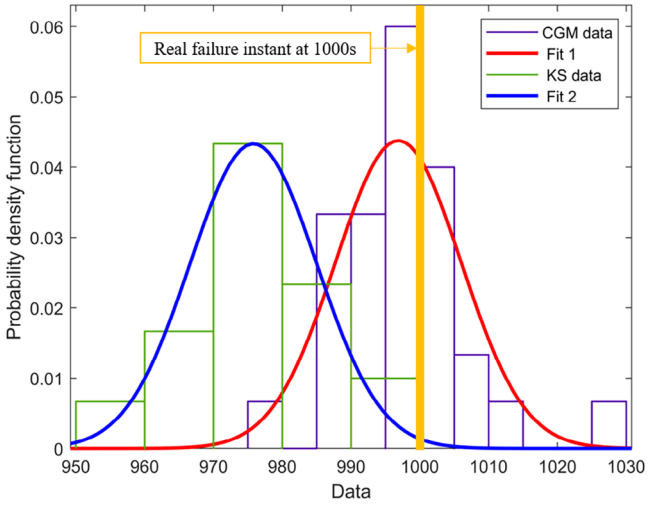

FIGURE 9 Histogram and PDF of the estimated $t^1_{\text{nok},1}$ over 30 simulations CGM (in red) and the KS method (in blue) with measurement noise $\sigma = 1°$.

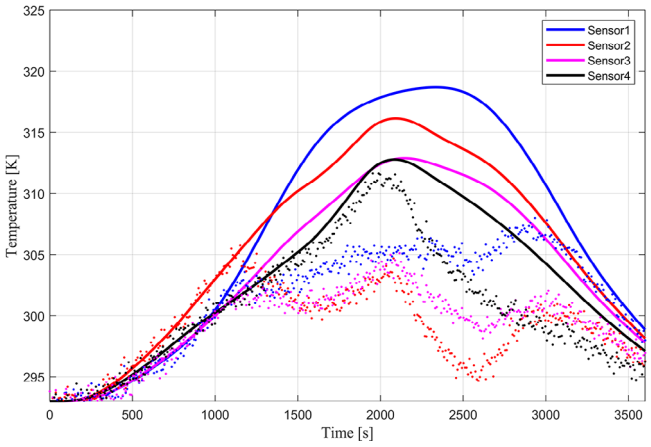

FIGURE 10 Sensor measurements: case when the source Φ_1 and Φ_1 fails with restart of the source Φ_1, represented as discrete points, without any failure and noise, represented as continuous data.

TABLE 6 Failure and restart times identification for Φ_1 and failure times for Φ_2.

		Instant $t^1_{\text{nok},1}$	Instant $t^2_{\text{nok},1}$	Instant $t^1_{\text{ok},1}$
$\sigma = 0.1°$C	CGM	997s (2.26)	1996.7s (2.23)	2498.7s (1.91)
	KS	1001.4s (1.4)	2005s (1, 4)	2504.5s (1.14)
$\sigma = 0.5°$C	CGM	996.5s (5.45)	1995s (5.75)	2499.3s (3.45)
	KS	999.5s (3.92)	2014s (5.15)	2513.8s (4.09)
$\sigma = 1°$C	CGM	999.46s (8.92)	1993s (10.45)	2494.4s (10.42)
	KS	976.7s (8.41)	2041.2s (6, 44)	2539.4s (5.68)

methods produce excellent outcomes. The results with the two approaches CGM and KS are obtained after 62 min and 40 min, respectively, on 30 simulations. We observe that the second approach yields results more rapidly. However, when the measurement noise of the sensors are increased, the failure instants of the two sources are well identified with the CGM approach than the second one KS with a high accuracy. The main disadvantages of this CGM approach is its computation time, which can be crucial depending on the problem's complexity.

5.2 | Identifying the failure and restart with source separation

After identifying the failure instants for two distinct sources using the two approaches, the challenge in this new scenario is to not only identify the failure instants, but also the restart (heating up again) of the sources. For this last configuration, we consider that first source fails at $t^1_{\text{nok},1} = 1000$ s then restarts at $t^1_{o\hat{k},1} = 2500$ s and the second source fails at $t^2_{\text{nok},1} = 2000$. For example, the measurements at the four sensors are given in Figure 10 with standard deviation $\sigma = 0.5°$. Using the same parameters as before, we obtain the results presented in Table 6, starting with the initialization $t^1_{\text{nok},1} = 500$ s, $t^1_{o\hat{k},1} = 1500$ s and $t^2_{\text{nok},1} = 1000$ s. The results with the two approaches GCM and KS are obtained after 68 min and 46 min, respectively, on 30 simulations.

In Table 6, it is clear that the two approaches have successfully identified the failure and restart instants. When the measurement noise is less significant, the two approaches give a good result, once the measurement noise is more important, the switching instants are slightly less well identified. The CGM approach gives a greater result to identify the switching instants and source separation, than the KS approach with better accuracy. In conclusion, the preceding table demonstrates that the two methods are applicable for identifying the failure and restart instants with source separation, particularly the CGM approach for this problem described by parabolic partial differential equations.

6 | CONCLUSION

This article presents a comprehensive analysis of failure and restart times identification in a physical system governed by linear parabolic partial differential equations. Two recent approaches are compared to provide a thorough assessment. The first approach, an original method formulated as a quadratic criterion minimization problem and solved using an iterative regularization method, demonstrates notable strengths and weaknesses. To evaluate its performance, a comparison is made with the second approach based on the Bayesian filter.

The comparative analysis reveals that the first approach exhibits superior accuracy in identifying failure and restart instants, even in the presence of significant measurement noise. This highlights the effectiveness of the proposed method. The CGM utilized in the first approach offers several advantages over traditional methods. It allows for the simultaneous identification of failures in multiple heating sources, a challenging task for conventional approaches. Additionally, the CGM

ensures numerical stability, resulting in efficient and precise computations. One disadvantage of the GCM approach is the computation time required for offline identification, which can be improved in the case of quasi-online identification.

There are several perspectives for future research following this work. First, the investigation can be extended to incorporate mobile sources and sensors, requiring relocation for more precise failures identification. In this context, decision support approaches based on pre-established scenarios can be developed. Finally, quasi-online approaches are well-suited for the examined conditions and can facilitate the development of backup solutions involving multiple mobile sources, particularly for online detection and identification.

NOMENCLATURE

Δt	time step, s
Δt_{obs}	time step of the observations, s
$\Delta x, \Delta y$	space step, m
λ	thermal conductivity, $W \cdot m^{-1} \cdot K^{-1}$
$\vec{n}$	unit external outward-pointing vector
ρc	volumetric heat, $J \cdot m^{-3} \cdot K^{-1}$
e	thickness, m
h	natural convection coefficient, $W \cdot m^{-2} \cdot K^{-1}$
T	temperature, K
t	time, s
t_f	final time, s
T_0	initial temperature, K
x	space variable, m
y	space variable, m

AUTHOR CONTRIBUTIONS

Mohamed Salim Bidou: Conceptualization; methodology; formal analysis; writing—original draft. **Laetitia Perez**: Validation; visualization; review & editing. **Sylvain Verron**: Validation; visualization; review & editing. **Laurent Autrique**: Validation; supervision; project administration.

CONFLICT OF INTEREST STATEMENT

The authors declare no conflicts of interest.

DATA AVAILABILITY STATEMENT

The data that support the findings of this study are available on request from the corresponding author.

ORCID

Mohamed Salim Bidou https://orcid.org/0000-0002-9157-9040

REFERENCES

1. Satyavada, H., Baldi, S.: A novel modelling approach for condensing boilers based on hybrid dynamical systems. Machines 4(2), 10 (2016)
2. Satyavada, H., Baldi, S.: Monitoring energy efficiency of condensing boilers via hybrid first-principle modelling and estimation. Energy 142, 121–129 (2018)
3. Cheng, M.B., Radisavljevic, V., Chang, C.C., Lin, C.F., Su, W.C.: A sampled-data singularly perturbed boundary control for a heat conduction system with noncollocated observation. IEEE Trans. Autom. Control 54(6), 1305–1310 (2009)
4. Wu, H.N., Li, H.X.: H_∞ fuzzy observer-based control for a class of nonlinear distributed parameter systems with control constraints. IEEE Trans. Fuzzy Syst. 16(2), 502–516 (2008)
5. Wu, H.N., Wang, J.W., Li, H.X.: Exponential stabilization for a class of nonlinear parabolic PDE systems via fuzzy control approach. IEEE Trans. Fuzzy Syst. 20(2), 318–329 (2011)
6. Krstic, M., Smyshlyaev, A.: Boundary Control of PDEs: A Course on Backstepping Designs. SIAM, Philadelphia, PA (2008)
7. Demetriou, M.A.: A model-based fault detection and diagnosis scheme for distributed parameter systems: A learning systems approach. ESAIM: Control Optim. Calculus Variat. 7, 43–67 (2002)
8. Ghantasala, S., El-Farra, N.H.: Robust actuator fault isolation and management in constrained uncertain parabolic PDE systems. Automatica 45(10), 2368–2373 (2009)
9. El-Farra, N.H., Ghantasala, S.: Actuator fault isolation and reconfiguration in transport-reaction processes. AlChE J. 53(6), 1518–1537 (2007)
10. Reppa, V., Tzes, A.: Fault detection and diagnosis based on parameter set estimation. IET Control Theory Appl. 5(1), 69–83 (2011)
11. Zhai, S., Wang, W., Ye, H.: Fault diagnosis based on parameter estimation in closed-loop systems. IET Control Theory Appl. 9(7), 1146–1153 (2015)
12. Chen, W., Saif, M.: Observer-based strategies for actuator fault detection, isolation and estimation for certain class of uncertain nonlinear systems. IET Control Theory Appl. 1(6), 1672–1680 (2007)
13. Han, Y., Oh, S., Choi, B., Kwak, D., Kim, H., Kim, Y.: Fault detection and identification of aircraft control surface using adaptive observer and input bias estimator. IET Control Theory Appl. 6(10), 1367–1387 (2012)
14. Cai, J., Ferdowsi, H., Sarangapani, J.: Model-based fault detection, estimation, and prediction for a class of linear distributed parameter systems. Automatica 66, 122–131 (2016). https://www.sciencedirect.com/science/article/pii/S0005109815005609.
15. Ferdowsi, H., Cai, J., Jagannathan, S.: Actuator and sensor fault detection and failure prediction for systems with multi-dimensional nonlinear partial differential equations. Int. J. Control Autom. Syst. 20(3), 789–802 (2022)
16. Feng, Y., Wang, Y., Wang, J.W., Li, H.X.: Backstepping-based distributed abnormality localization for linear parabolic distributed parameter systems. Automatica 135, 109930 (2022). https://www.sciencedirect.com/science/article/pii/S0005109821004544
17. Lei, Y., Li, J., Zhao, A.: Spatiotemporal fault detection, estimation and control for nonlinear reaction-diffusion equations. Appl. Math. Comput. 418, 126859 (2022)
18. Ferdowsi, H., Cai, J., Jagannathan, S.: Filter-based fault detection and isolation in distributed parameter systems modeled by parabolic partial differential equations. IEEE Access 11, 45011–45027 (2023)
19. Bidou, M.S., Perez, L., Verron, S., Autrique, L.: Identification of failure times for a system governed by a non-linear parabolic partial differential equation. IFAC-PapersOnLine 55(40), 37–42 (2022). https://www.sciencedirect.com/science/article/pii/S2405896323000502
20. Tikhonov, A.N.: On the solution of ill-posed problems and the method of regularization. In: Doklady Akademii Nauk, vol. 151, pp. 501–504. Russian Academy of Sciences, Moscow (1963)
21. Yang, F., Fu, C.L.: A simplified Tikhonov regularization method for determining the heat source. Appl. Math. Modell. 34(11), 3286–3299 (2010)
22. Beck, J.V.: Nonlinear estimation applied to the nonlinear inverse heat conduction problem. Int. J. Heat Mass Transfer 13(4), 703–716 (1970). https://www.sciencedirect.com/science/article/pii/001793107090044X
23. Blanc, G., Beck, J.V., Raynaud, M.: Solution of the inverse heat conduction problem with a time-variable number of future temperatures. Numer. Heat Transfer, Part B: Fund. 32(4), 437–451 (1997). https://doi.org/10.1080/10407799708915018
24. Özisik, M.N., Orlande, H.R.: Inverse Heat Transfer: Fundamentals and Applications. CRC Press, Boca Raton, FL (2021)

25. Givoli, D.: A tutorial on the adjoint method for inverse problems. Computer Meth. Appl. Mech. Eng. 380, 113810 (2021). https://www.sciencedirect.com/science/article/pii/S0045782521001468
26. Yin, M., Zheng, X., Humphrey, J.D., Karniadakis, G.E.: Non-invasive inference of thrombus material properties with physics-informed neural networks. Comput. Methods Appl. Mech. Eng. 375, 113603 (2021). https://www.sciencedirect.com/science/article/pii/S004578252030788X
27. Patel, D.V., Ray, D., Oberai, A.A.: Solution of physics-based Bayesian inverse problems with deep generative priors. Comput. Methods Appl. Mech. Eng. 400, 115428 (2022). https://www.sciencedirect.com/science/article/pii/S004578252200473X
28. Yang, F., Yan, L., Wei, T.: The identification of a Robin coefficient by a conjugate gradient method. Int. J. Numer. Methods Eng. 78(7), 800–816 (2009)
29. Lu, T., Han, W., Jiang, P., Zhu, Y., Wu, J., Liu, C.: A two-dimensional inverse heat conduction problem for simultaneous estimation of heat convection coefficient, fluid temperature and wall temperature on the inner wall of a pipeline. Prog. Nucl. Energy 81, 161–168 (2015)
30. Huang, C.H., Wang, S.P.: A three-dimensional inverse heat conduction problem in estimating surface heat flux by conjugate gradient method. Int. J. Heat Mass Transfer 42(18), 3387–3403 (1999). https://www.sciencedirect.com/science/article/pii/S0017931099000204
31. Vergnaud, A., Perez, L., Autrique, L.: Adaptive selection of relevant sensors in a network for unknown mobile heating flux estimation. IEEE Sens. J. 20(24), 15133–15142 (2020)
32. He, Z., Ni, F., Wang, W., Zhang, J.: A physics-informed deep learning method for solving direct and inverse heat conduction problems of materials. Mater. Today Commun. 28, 102719 (2021). https://www.sciencedirect.com/science/article/pii/S235249282100711X
33. Alifanov, O.M.: Iterative regularization of inverse problems. Inverse Heat Transfer Problems. In: International Series in Heat and Mass Transfer, pp. 227–328. Springer, Berlin, Heidelberg (1994). https://doi.org/10.1007/978-3-642-76436-3_9
34. Bidou, M.S., Verron, S., Perez, L., Autrique, L.: Kalman smoother for detection of heat sources defects. In: 2022 International Conference on Control, Automation and Diagnosis (ICCAD), pp. 1–6. IEEE, Piscataway (2022)
35. Vergnaud, A., Perez, L., Autrique, L.: Quasi-online parametric identification of moving heating devices in a 2D geometry. Int. J. Therm. Sci. 102, 47–61 (2016)
36. Ashby, M.F., CEBON, D.: Materials selection in mechanical design. Le J. Phys. IV 3(C7), C7–1 (1993)
37. Lascoup, B., Perez, L., Autrique, L.: Defect localization based on modulated photothermal local approach. Comp. Part B: Eng. 65, 109–116 (2014)
38. Jarny, Y., Ozisik, M.N., Bardon, J.P.: A general optimization method using adjoint equation for solving multidimensional inverse heat conduction. Int. J. Heat Mass Transfer 34(11), 2911–2919 (1991). https://www.sciencedirect.com/science/article/pii/0017931091902519
39. Perez, L., Autrique, L., Gillet, M.: Implementation of a conjugate gradient algorithm for thermal diffusivity identification in a moving boundaries system. J. Phys.: Conf. Ser. 135, 012082 (2008)
40. Beddiaf, S., Perez, L., Autrique, L., Jolly, J.C.: Parametric identification of a heating mobile source in a three-dimensional geometry. Inverse Prob. Sci. Eng. 23(1), 93–111 (2015). https://doi.org/10.1080/17415977.2014.890608
41. Beddiaf, S., Perez, L., Autrique, L., Jolly, J.C.: Simultaneous determination of time-varying strength and location of a heating source in a three-dimensional domain. Inverse Prob. Sci. Eng. 22(1), 166–183 (2014). https://doi.org/10.1080/17415977.2013.828054
42. Morozov, V.A.: Methods for Solving Incorrectly Posed Problems. Springer Science & Business Media, New York (2012)
43. Kaipio, J., Somersalo, E.: Statistical and Computational Inverse Problems. Applied Mathematical Sciences. Springer, New York (2006). https://books.google.fr/books?id=h0i-Gi4rCZIC
44. Kaipio, J.P., Fox, C.: The Bayesian framework for inverse problems in heat transfer. Heat Transfer Eng. 32(9), 718–753 (2011). https://doi.org/10.1080/01457632.2011.525137
45. Özişik, M.N., Orlande, H.R., Colaco, M.J., Cotta, R.M.: Finite Difference Methods in Heat Transfer. CRC Press, Boca Raton, FL (2017)
46. Murphy, K.P.: Machine Learning: A Probabilistic Perspective. MIT Press, Cambridge, MA (2012)
47. Rauch, H.E., Tung, F., Striebel, C.T.: Maximum likelihood estimates of linear dynamic systems. AIAA J. 3(8), 1445–1450 (1965)
48. Gaaloul, N., Daouas, N.: An extended approach of a Kalman smoothing technique applied to a transient nonlinear two-dimensional inverse heat conduction problem. Int. J. Therm. Sci. 134, 224–241 (2018)
49. Wen, S., Qi, H., Niu, Z.T., Wei, L.Y., Ren, Y.T.: Efficient and robust prediction of internal temperature distribution and boundary heat flux in participating media by using the Kalman smoothing technique. Int. J. Heat Mass Transfer 147, 118851 (2020)

How to cite this article: Bidou, M.S., Perez, L., Verron, S., Autrique, L.: A model-based failure times identification for a system governed by a 2D parabolic partial differential equation. IET Control Theory Appl. 1–13 (2024). https://doi.org/10.1049/cth2.12652